sciendo

POLISH MARITIME RESEARCH 2 (102) 2019 Vol. 26; pp. 163-172
10.2478/pomr-2019-0036

NUMERICAL PREDICTION OF PROPELLER-HULL INTERACTION CHARACTERISTICS USING RANS METHOD

Tran Ngoc Tu
Do Duc Luu
Nguyen Thi Hai Ha
Nguyen Thi Thu Quynh
Nguyen Minh Vu
Vietnam Maritime University, Hai Phong City, Vietnam

ABSTRACT

The paper presents the results of computational evaluation of the hull-propeller interaction coefficients, also referred to propulsive coefficients, based on the unsteady RANS flow model. To obtain the propulsive coefficients, the ship resistance, the open-water characteristics of the propeller, and the flow past the hull with working propeller were computed. For numerical evaluation of propeller open-water characteristics, the rotating reference frame approach was used, while for self-propulsion simulation, the rigid body motion method was applied. The rotating propeller was modelled with the sliding mesh technique. The dynamic sinkage and trim of the vessel were considered. The free surface effects were included by employing the volume of fluid method (VOF) for multi-phase flows. The self-propulsion point was obtained by performing two runs at constant speed with different revolutions. The well-known Japan Bulk Carrier (JBC) test cases were used to verify and validate the accuracy of the case studies. The solver used in the study was the commercial package Star-CCM+ from SIEMENS.

Keywords: Propeller, interaction, hull, wake fraction, thrust deduction, relative rotative efficiency, RANS equations

INTRODUCTION

In assessing the performance of the propeller working behind the ship hull plays an important role in the design process and it is still one of the most demanding challenges in computational ship hydrodynamics. The interaction between the propeller and the ship comprises wake fraction, thrust deduction, and relative rotative efficiency. Correct design of the ship propulsion system depends on the accuracy in determining those components.

Nowadays, scale model tests still provide the most accurate data for hull-propeller interaction. However, these tests are both time-consuming and cost–intensive with respect to both model manufacturing and the experiment itself. Thus, this method is impractical generally for hydrodynamics optimization studies, especially those involving hull-propeller interaction.

Computational Fluid Dynamics (CFD) has made a remarkable progress in the past few decades in the field of ship hydrodynamics. With the development of computational resources, CFD methods have been widely applied in practical ship designing and performance predictions. They provide relatively accurate results, and are relatively fast and inexpensive, compared to the experimental data. Moreover, they provide the visualization of flow quantities, i.e. pressure and velocity, the latter in the form of contour maps, vector maps, and streamlines, which may often allow the designers to develop or improve their design. The group of CFD methods used to solve hydrodynamics problems includes: potential flow theory (panel code), Reynold Averaged Navier-Stokes (RANS) equations, and Large Eddy Simulation (LES). At the moment, the most popular approach is the RANS method, as it provides a sufficient accuracy for engineering purposes at reasonable computational time [1]. Thus, this paper uses the RANS method for evaluating the hull-propeller interaction coefficients.

Some useful results using the RANS method for simulation of propeller-hull interaction have been already achieved. Villa

Fig. 1. JBC geometry for simulations of case study "ship resistance" (top) and case study "self-propulsion" in calm water (bottom)

et al. [2], Pacuraru et al. [3] and Win et al. [4] used this method in combination with the actuator disk method, instead of the actual propeller, to perform the self-propulsion simulation. That approach allowed the authors to avoid complexities associated with moving meshes and to achieve, as a result, shorter run times. However, the applied method could not provide the detailed flow field around the propeller. Bugalski et al. [5] used the RANS method together with the rigid body motion method (actual rotating propeller) to simulate the self-propulsion. The dynamic sinkage and trim of the vessel were not considered. That approach helped to avoid the uncertainties caused by the dynamic fluid body interaction (DFBI) model used to simulate the ship's behaviour with the hull free to move in the pitch and heave directions, and thus to accelerate the simulation convergence. Bekhit [6] used the RANS method to study self-propulsion of the Japan Bulk Carrier (JBC) ship model using the body force propeller method and the fully discretized propeller model. The results of that study have shown that the propeller model provides efficient and reliable results, and that the flow characteristics and blade pressure distributions can be fully visualized. However, it takes a significant computational time, and both modelling and computations themselves are more complex in comparison with the body force propeller method. Seo et al. [7] and Gokce et al. [8] used the RANS method to simulate ship resistance, and propeller open-water and self-propulsion characteristics in order to evaluate the hull-propeller interaction coefficients. Seo et al. focused on flexible meshing techniques, while the base of choice for computational domain, time step, y+ value, and mesh convergence was not considered, although these are the key issues determining the numerical accuracy. In the study by Gokce et al., the discrepancy between computed and experimental results of open-water propeller performance was especially sound at higher advance coefficients.

The abovementioned literature has played an important role for further researches using the RANS method to assess the performance of a propeller working behind the ship hull. In the research reported in this paper, the ship resistance, the propeller open-water characteristics, and the thrust/torque characteristics behind the ship hull were computed to obtain the coefficients of hull-propeller interaction. For this purpose, the RANS method with Star-CCM+ solver was used. The ship resistance was computed for the hull free to sink and trim. In the computations of propeller open-water characteristics, the rotating reference frame was used. This approach, consisting in considering additional terms in the momentum equation, is fully suitable for open-water analyses and its results are fully equivalent to the case of actual propeller rotation, while the computational time is reduced and the convergence is faster, as physical motion of the computational mesh can be avoided [9]. For the self-propulsion simulation, the rigid body motion method was applied. The rotating propeller was modelled with the sliding mesh technique. The dynamic sinkage and trim of the vessel were considered. The base of choice for computational domain, time step, y+ value, and mesh convergence was considered in this study. The case study used to verify and validate the computational model was the well-known JBC ship model; the geometry of which and the experimental data for validation are available on the website of the Workshop on CFD in Ship Hydrodynamics, Tokyo 2015 [10], [11].

NUMERICAL SIMULATION

GEOMETRY AND CONDITIONS

Ship and propeller geometry

The JBC is a hypothetical modern bulk carrier designed and tested experimentally to provide data for both exploration of flow physics and CFD validation. The data of ship resistance, propeller open water characteristics, and self-propulsion characteristics in model scale ($\lambda = 40$) are available in [10], [11].

The JBC hull and propeller geometry are shown in Fig.1. and Fig. 2, while its dimensions and geometrical properties are listed in Table 1 and Table 2.

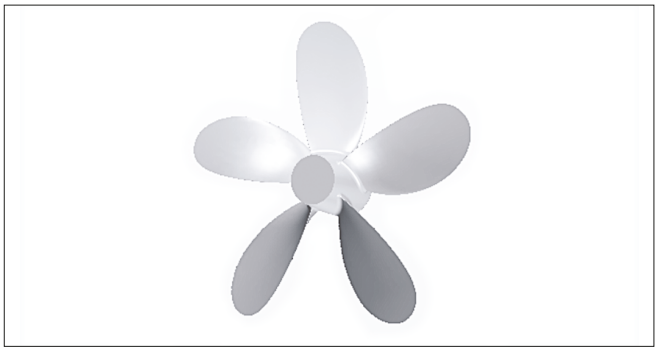

Fig. 2. JBC propeller geometry for case study "propeller open-water simulation"

Tab. 1. Main particulars of JBC [10]

Descriptions		Full scale	Model
Scale factor	λ	–	40
Length between perpendiculars	L_{PP} (m)	280.00	7.00
Length of waterline	L_{WL} (m)	285.00	7.125
Breadth	B (m)	45.00	1.125
Draft	T (m)	16.5	0.4125
Volume	∇ (m^3)	17837	2.7870
Wetted surface	S (m^2)	19556	12.222
Longitudinal Centre of Buoyancy From Midship	LCB (%L_{PP}), fwd+	2.5475	
Propeller centre, long. location (from FP)	x/L_{PP}	0.985714	
Propeller centre, vert. location (bellow WL)	$-z/L_{PP}$	−0.0404214	
Propeller rotation direction (view from stern)	–		

Tab. 2. Propeller principal particulars [10]

Descriptions		Unit	Value
Diameter	D	m	0.203
Blade area ratio	A_E/A_0	–	0.5
Hub ratio	D_h/D	–	0.18
Number of blades	Z	–	5
Pitch ratio	$P_{0.7}/D$		0.75
Direction of rotation	–	–	Right-handed

Test case conditions

For the case studies (1) "ship resistance" and (3) "self-propulsion", the computations were performed for the design draft T = 0.4125 m, corresponding to the hull displacement volume ∇ = 2.7870 m^3, and for Froude number Fr = 0.142 and Reynolds number Re = $7.46.10^6$.

The settings used in the ship resistance simulation correspond to case 1.1a according to [11], i.e.:

- Calm water condition;
- Without rudder and Energy Saving Device (ESD), without propeller;
- The vessel is free to trim and sink.

The settings used in the self-propulsion simulation correspond to case 1.5a according to [11] i.e.:

- Calm water condition;
- Without rudder and ESD, with propeller;
- The vessel is free to trim and sink.

The case study (2) "propeller open water simulation" was carried out for the same conditions as the experiment labelled as 'case 1.5a' according to [11]. A number of simulations were carried out for different advance coefficients J which varied from 0.4 to 0.8 (to reflect the typical propeller operation range) with the step equal to 0.1. The propeller revolutions were kept constant and equal to n=20 rps, and J was changed by changing the advance velocity.

The water parameters for all three case studies corresponded to the values recorded in the experiment: water density ρ = 998.2 kg/m^3, water kinematic viscosity ν = $1.1070x10^{-6}$ m^2/s) [11].

COMPUTATIONAL SETUP

COMPUTATIONAL DOMAIN AND BOUNDARY CONDITIONS

The commercial package Star-CCM+ from SIEMENS was used for the computations.

For case (1) "ship resistance", one half of the hull was considered due to flow symmetry, while in case (3) "self-propulsion", the entire ship hull with propeller was analysed.

Based on the recommendations given by ITTC [12] and sample settings provided in the software documentation [13], the dimensions of the computational domain built around the ship hull for case (1) were as follows: the inlet boundary was located at a distance of 1.5Lpp from FP, the outlet boundary at 2.5Lpp behind AP, and the bottom and top boundaries at 2.5Lpp and 1.25Lpp from the free surface, respectively. The lateral boundary was located 2.5Lpp from the hull symmetry plane.

For case (2) "propeller open water simulation", the computational domain was cylindrical and characterized by the following dimensions, expressed as multiples of propeller diameter D: the inlet was located 3D from the midpoint of the chord of the root section, while the outlet ant the outer boundaries were located 4D from the propeller plane and the propeller axis, respectively. It should be noted that the locations of boundaries were selected based on the applications reported in studies [14] and recommendations given by ITTC [15].

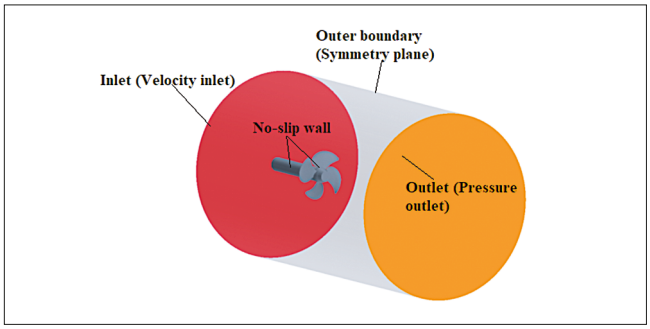

Fig. 3. Computational domain and boundary conditions in propeller open water simulation

For the self-propulsion simulation, the computational domain was divided into two regions: the stationary region surrounding the whole modelled system, and the rotating sub-region having the form of a cylinder surrounding the propeller (see Fig. 8).

Regarding the boundary conditions – for cases (1) and (3), the prescribed velocity conditions were used at inlet, top

and bottom. The no-slip wall condition was applied on hull and propeller surfaces. At outlet, the hydrostatic pressure was specified. The slip wall condition was used on the side walls. The free surface was located at z = 0. The ship stern (aft perpendicular) was located at x = 0. For case (2), the velocity condition was used at inlet and the pressure condition at outlet. The symmetry plane condition was used at outer boundary. The no-slip wall condition was used on propeller, hub and shaft surfaces (Fig. 3).

Mesh generation

The mesh used for all three case studies was the hexahedral mesh.

For case study (1), to avoid using fine mesh resolution where unnecessary, local volume refinement was applied at bow and stern. To capture the exact flow behaviour near the walls, prism layers were used. Moreover, to resolve the flow around the hull near the free surface, a finer mesh was created in the free surface region. The average Y+ value on the submerged part of the hull was 50 (Fig. 4). The mesh generated for case study (1) is shown in Fig. 5.

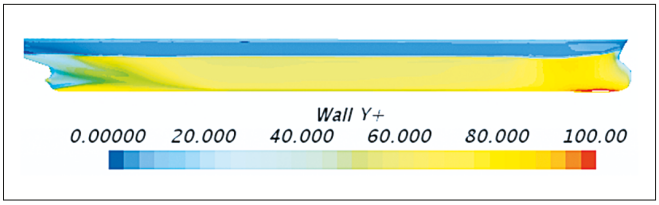

Fig. 4. Y+ value on hull surface

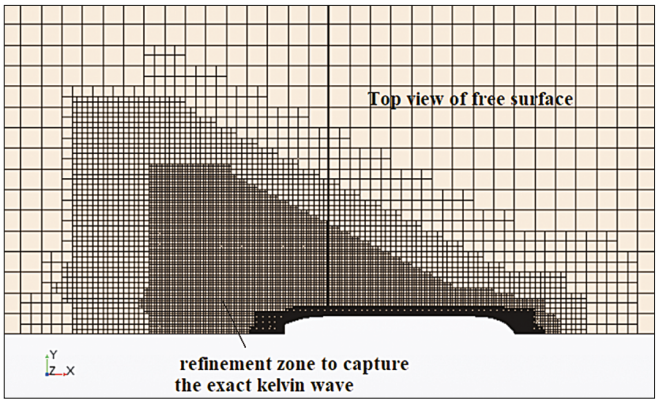

Fig. 5. Mesh structure for ship resistance simulation

For case study (2), to avoid using fine mesh resolution where unnecessary, i.e. at large distance from the propeller, local refinement was applied around the propeller. Moreover, the regions of leading edge, trailing edge and tip of propeller blades were further refined due large curvature of the blade surface in these regions [5]. To resolve the boundary layer, the prism layer was used. In mesh generation, the dimensionless normal distance y^+ of the first cell layer adjacent to the wall was kept well below 5 to resolve the near wall boundary layer. Such a range corresponds to the viscous sublayer in the model scale simulation [16]. The mesh generated for this case is shown in Fig. 7.

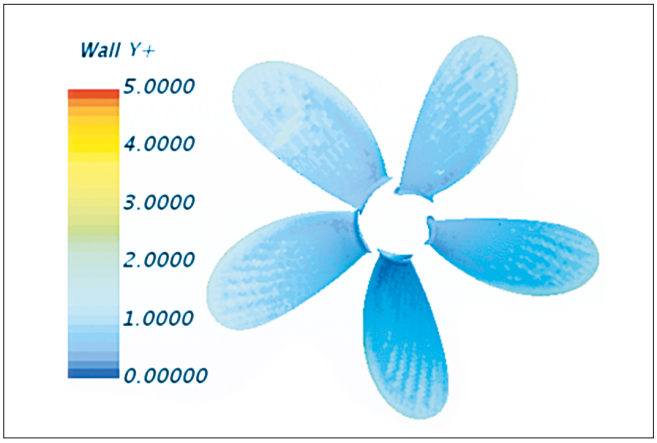

Fig. 6. Y+ value on propeller blades

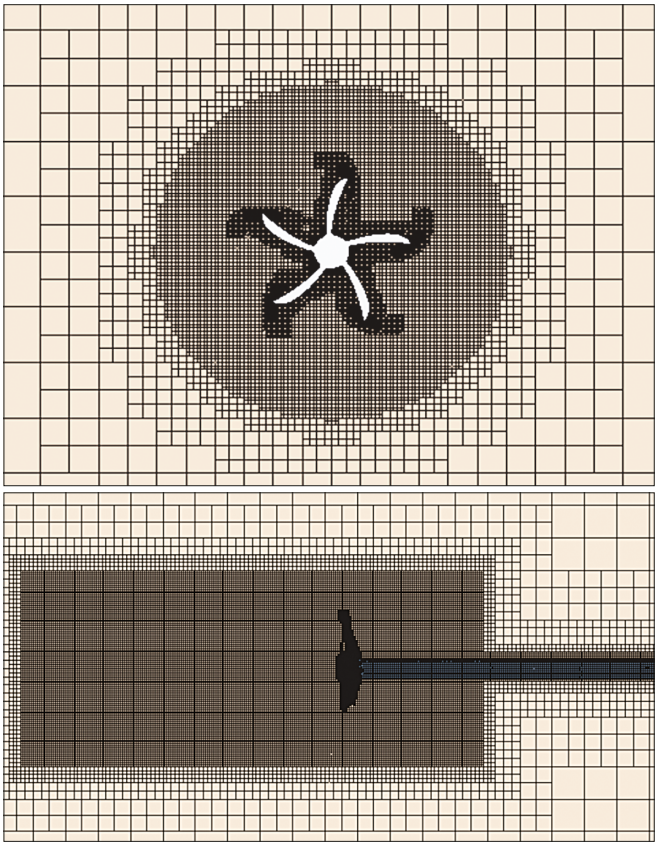

Fig. 7. Mesh structure for open water simulation

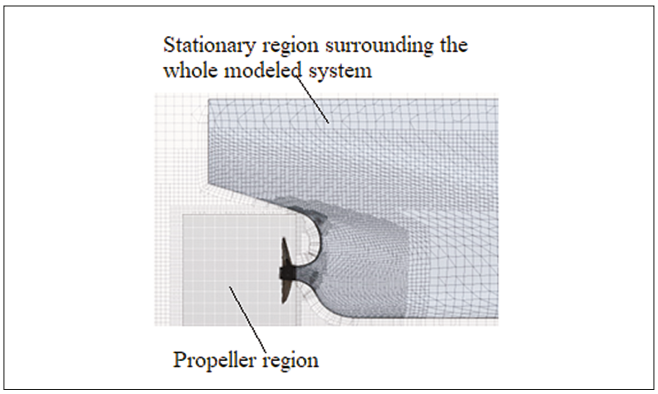

Fig. 8. Mesh structure for self-propulsion simulation

For case study (3), the mesh setup for the ship and propeller regions was the same as for cases (1) and (2). The refined mesh was used near the stern region surrounding the propeller to capture properly the wake field. The sliding mesh technique was used for the rotating propeller.

Physical model

The computation was carried out using the Reynolds Averaged Navier-Stokes (RANS) equations. The turbulence model used in all three case studies was SST K-omega [12].

- For the propeller open-water analysis, the propeller inflow was uniform, so the steady RANS equations with the rotating reference frame were used. This approach is fully equivalent to the case of actual propeller rotation, while the computational time is reduced and the convergence is faster, as physical motion of the computational mesh is avoided [9].
- For ship resistance computations, the 6-DOF motion and the VOF multiphase model were employed to handle running trim, sinkage, and the free surface wave flow around the hull. The hull motion was captured during the computation by using the DFBI Equilibrium option, i.e. the dynamic fluid-body interaction motion solver optimized for fast heading towards the steady state solution (Y-axis rotation and Z-direction motion was allowed for the hull). Wave damping in the region beginning about 0.5L away from the hull was applied to reduce the resistance force fluctuation due to wave reflections within the domain.
- In the case of propeller working behind the ship, the rigid body motion method was applied. The propeller rotation was introduced by the DFBI Superposed Rotation model (it superimposes an additional fixed body rotation onto the DFBI motion, thus making it possible to model a propeller attached to the ship [13]).

Choice of time step

One of the key issues determining the numerical accuracy is choosing the time step size. For resistance computations, the time step is the function of ship's length and speed, according to the ITTC equation [12]:

$$\Delta t = 0.005 \sim 0.01 L/\mathrm{V} \tag{1}$$

where V and L are the ship's speed and length, respectively.

For the self-propulsion simulation, according to the ITTC recommendation [15], the time step was selected such that the propeller rotation angle was one degree per time step.

RESULTS AND DISCUSSION

MESH DEPENDENCY STUDY

One of key issues determining the numerical accuracy is mesh dependency. Due to finite size of the finite-volume cells, some discretization errors appear, being the difference between the solution of the difference equations and the exact (continuum) solution of the differential equations. It is important to know the magnitude of these discretization errors and to ensure that the used mesh is fine enough to reduce the error to an acceptable level [17]. In the present case, the mesh sensitivity study has been conducted using three meshes with non-integer mesh refinement ratio $r_G = \sqrt{2}$ (the value recommended by ITTC [18]) so that the coarse, medium, and fine mesh corresponded to the cell number of 0.696, 1.315 and 2.845 million cells, respectively, for the ship resistance study, and to 0.852, 1.568 and 3.7 million cells for the propeller open-water simulation at advance coefficient J = 0.5.

Mesh refinement was done by reducing the cell size in all directions outside the prism layer. The idea here was to keep the same y+ values at near-wall cells for all three cases.

The mesh sensitivity study was performed by comparing the quantities recorded in the experiment (EFD), denoted as D and treated as reference values, with the corresponding S values obtained from CFD:

$$E\%D = \frac{(D-S)}{D}.100\% \tag{2}$$

Changes between the simulations performed for two different meshes, i.e. fine-medium ε_{12} and medium-coarse ε_{23}, are defined as follows:

Tab. 3. Ship resistance at Fr=0.142 for different meshes

Parameter		EFD (D) [11]	V&V Study			ε_{32} %	ε_{12} %
			Mesh#3	Mesh#2	Mesh#1		
$C_T x10^3$	Value	4.289	4.392	4.370	4.350	–0.50	–0.46
	E%D	/	–2.401	–1.889	–1.421	/	/
$C_F x10^3$	Value	/	3.112	3.150	3.161	1.21	0.35
	E%D	/	/	/	/	/	/
$C_P x10^3$	Value	/	1.280	1.220	1.189	–4.92	–2.61
	E%D	/	/	/	/	/	/

$$\varepsilon_{12} = (S_1 - S_2)/ S_1; \varepsilon_{23} = (S_2 - S_3)/ S_2 \quad (3)$$

The results of the mesh dependency study for ship resistance and propeller open-water simulations are illustrated in 0 and 0, respectively. In the present case, a tendency to converge in both case studies was observed for the considered meshes, i.e. the resulting resistance coefficient and the propeller characteristics changed monotonically with mesh density (the solution change between meshes 1 and 2 (ε_{12}) was smaller than that between meshes 2 and 3 (ε_{23}), and the solution changes between meshes 1 and 2 (ε_{12}), were very small for all case studies). Besides, the comparison has shown quite good agreement between simulation (CFD) and experimental values (EFD), especially for the fine mesh (the errors of CT for fine meshes were less than 1.5% for ship resistance and propeller open water predictions), so the fine mesh was used in further studies of propeller open-water and self-propulsion simulations.

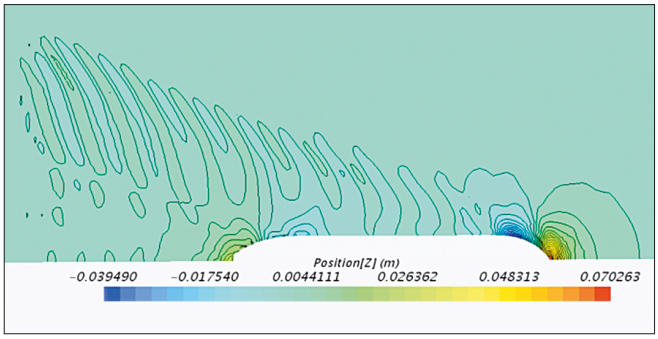

Fig. 9. Wave elevation contour plot [Mesh 1]

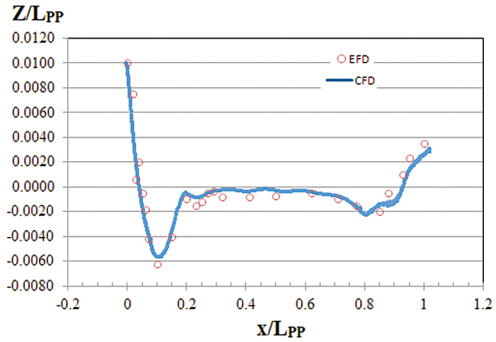

Fig. 10. Comparison of wave profile

The wave pattern for fine mesh is presented in Fig.9. The wave profiles along the hull surface are compared in Fig.10. The wave obtained from CFD shows good agreement with the experimental data.

Results of open-water propeller simulation

The comparison between the calculated and measured values of the open-water propeller characteristics shown in Table 5 shows that good agreement has been achieved.

Results of self-propulsion simulations

The self-propulsion simulations were performed using the fine mesh for both the hull and the propeller. Unlike in the resistance computations, here both sides of the hull were modelled directly. The total number of mesh elements was 6.8 million cells (4.2 million cells for the stationary region

Tab. 4. Results of mesh independency study at advance coefficient J=0.5

Parameter		EFD (D) [11]	V&V Study			ε_{32} %	ε_{12} %
			Mesh#3	Mesh#2	Mesh#1		
K_T	Value	0.1798	0.181	0.1805	0.1803	–0.28	–0.11
	E%D	/	–0.67	–0.39	–0.28	/	/
K_Q	Value	0.2479	0.2413	0.243	0.2445	0.70	0.61
	E%D	/	2.66	1.98	1.37	/	/
η_0	Value	0.5771	0.597	0.591	0.587	–0.98	–0.73
	E%D	/	–3.43	–2.43	–1.68	/	/

Tab. 5. Open-water simulation results vs. experimental data

J	K_T			$10K_Q$			η_0		
	EFD [11]	CFD	E%D [%]	EFD [11]	CFD	E%	EFD [11]	CFD	E%D [%]
0.4	0.2214	0.227	–2.47	0.2871	0.281	2.12	0.4909	0.5143	–4.8
0.5	0.1798	0.1803	–0.28	0.2479	0.2445	1.37	0.5771	0.5868	–1.7
0.6	0.1349	0.1358	–0.66	0.2027	0.203	–0.15	0.6354	0.6388	–0.5
0.7	0.0867	0.0905	–4.20	0.1509	0.154	–2.05	0.64	0.6547	–2.3
0.8	0.0353	0.0371	–4.85	0.0921	0.0905	1.74	0.4879	0.5220	–7.0

surrounding the whole modelled system, and 2.6 million cells for the rotating sub-region surrounding the propeller). The hull was free to trim and sink. Propeller rotation was introduced by using the DFBI Superposed rotation model.

The self-propulsion computations were performed at ship self-propulsion point, where the rate of propeller revolutions n was adjusted to obtain force equilibrium (thrust/drag balance). In practice, it is difficult to obtain this condition in one run, and a common practice is to carry out at least two constant-speed runs with different revolutions, hence the discrepancy between the total self-propulsion resistance RT(SP) and the thrust of the propeller working behind the ship T equals zero. The model simulations considered the applied towing force (Skin Friction Correction, SFC [19], which takes into account the difference in skin friction coefficients between the model and the full scale ship):

$$T = R_{T(SP)} - SFC \tag{4}$$

where SFC = 18.2 N, (the value computed from experimental data [11]).

The computed results of ship's thrust and resistance versus propeller revolutions are shown in Table 6 and in Fig. 111 for the velocity of 1.179 m/s. The self-propulsion point was searched using linear interpolation, and the obtained rotational speed 2 was n = 7.88 *rps* (see Fig. 11).

Tab. 6. Calculated results of two rps cases

n [rps]	$R_{T(SP)}$ – SFC [N]	T [N]	$10K_{Q(SP)}$
7.7	22.4	21.9	0.283
7.9	23.47	23.52	0.289

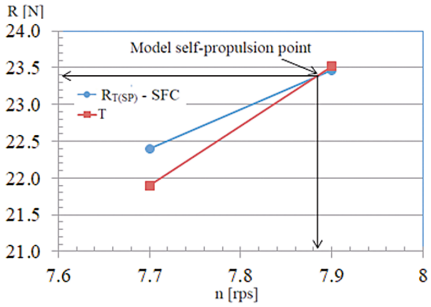

Fig. 11. Model self-propulsion point

Based on the computed self-propulsion point, the propulsive coefficients were determined as follow:

The thrust deduction t is given by the following formula [19]:

$$t = \frac{T + SFC - R_T}{T} \tag{5}$$

where R_T is the total ship resistance without propeller working behind the ship.

The effective wake fraction w_T and the relative rotative efficiency η_R were obtained using thrust identity with the open water propeller results (see Fig. 14) from Fig.12. The wake fraction is given by the following formula [20]:

$$w_T = 1 - \frac{J_0}{J_{SP}} \tag{6}$$

while the relative rotative efficiency is given by [20]:

$$\eta_R = \frac{K_{Q0}}{K_{Q(SP)}} \tag{7}$$

where J_0 and K_{Q0} are the advance and torque coefficients, respectively, obtained from the open-water propeller characteristics – Fig. 12, while J_{SP} and $K_{Q(SP)}$ are the advance and torque coefficients obtained from the self-propulsion simulation.

Table 7 compares the self-propulsion parameters obtained from the computation with the experimental data taken from [11]. Good agreement between these two data is observed.

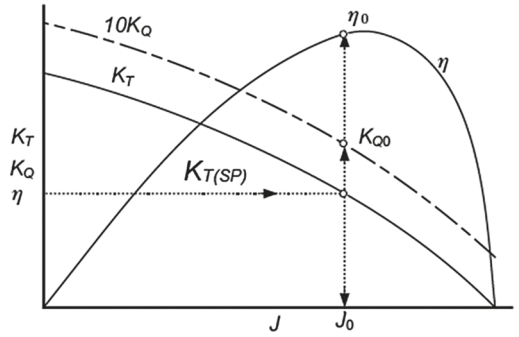

Fig. 12. Open-water curve and thrust identity [20]

Tab. 7. Comparing computed propeller-hull interaction results with experimental data

Parameter	EFD (D)	CFD (S)	E%D
$R_{T(SP)}$ [N]	40.79	41.60	–1.99
$R_{P(SP)}$ [N]	–	14.72	–
$R_{F(SP)}$ [N]	–	26.88	–
R_T [N]	36.36	36.88	–1.43
R_P [N]	–	10.08	–
R_F [N]	–	26.8	–
n [rps]	7.8	7.88	–1.03
T [N]	22.56	23.4	–3.72
$K_{T(SP)}$	0.217	0.222	–2.45
$K_{Q(SP)}$	0.0279	0.0288	–3.23
K_{Q0}	0.0283	0.0293	–3.53
SFC	18.2	18.2	0.00
J_0	0.408	0.405	0.74
J_{SP}	0.745	0.737	1.02
t	0.109	0.113	–4.47
w	0.452	0.451	0.34
η_R	1.014	1.017	–0.298

The distributions of the flow quantities: velocity and pressure, in the stern region and over the propeller's blade surface are shown in Fig. 13, Fig. 14 and Fig. 16.

As can be seen, the wake behind the ship strongly influences the propeller, and the propeller also influences the ship flow.

The influence of the propeller on the ship flow can be clearly observed in the pressure field. The propeller accelerates the flow ahead of it, thus reducing the pressure on the aft part of the hull (Fig. 13 and Fig. 14) and increasing the pressure resistance. The value of pressure resistance in the self-propelled condition is 1.46 times as large as that of the hull without propeller (see Table 7).

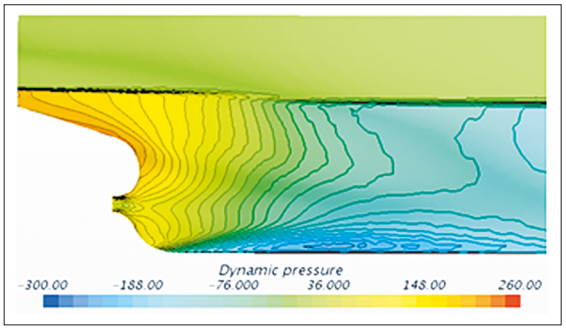

Fig. 13. Dynamic pressure contours on hull surface in ship resistance case

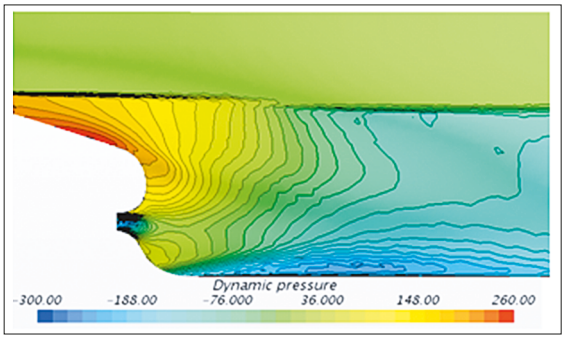

Fig. 14. Dynamic pressure contours on hull surface in self-propulsion case

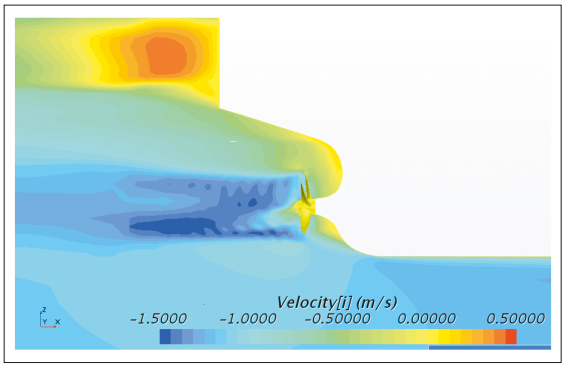

Fig. 15. Axial velocity field in symmetry plane

Due to the hull shape curvature in the aft part and the boundary layer development effects, the wake structure and its influence on the propeller are non-uniform, which can be clearly observed in the axial velocity field behind the propeller (Fig. 15). The asymmetric velocity distribution is expected to occur as the effect of different pressure distributions on individual propeller blades, both on their suction and pressure sides (Fig. 16).

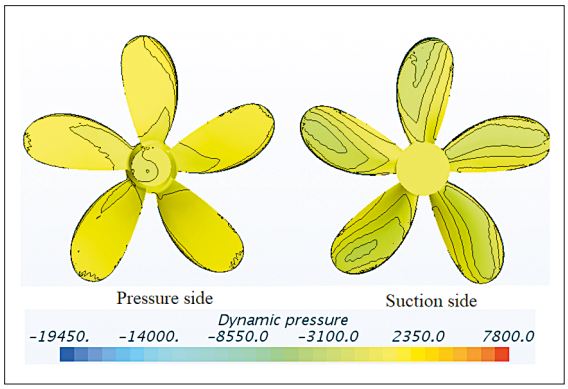

Fig. 16. Dynamic pressure contours on propeller blade surfaces in self-propulsion case

The computed axial velocity distributions are compared in Fig. 17 and Fig. 18 with the measured values for the case without and with propeller, respectively.

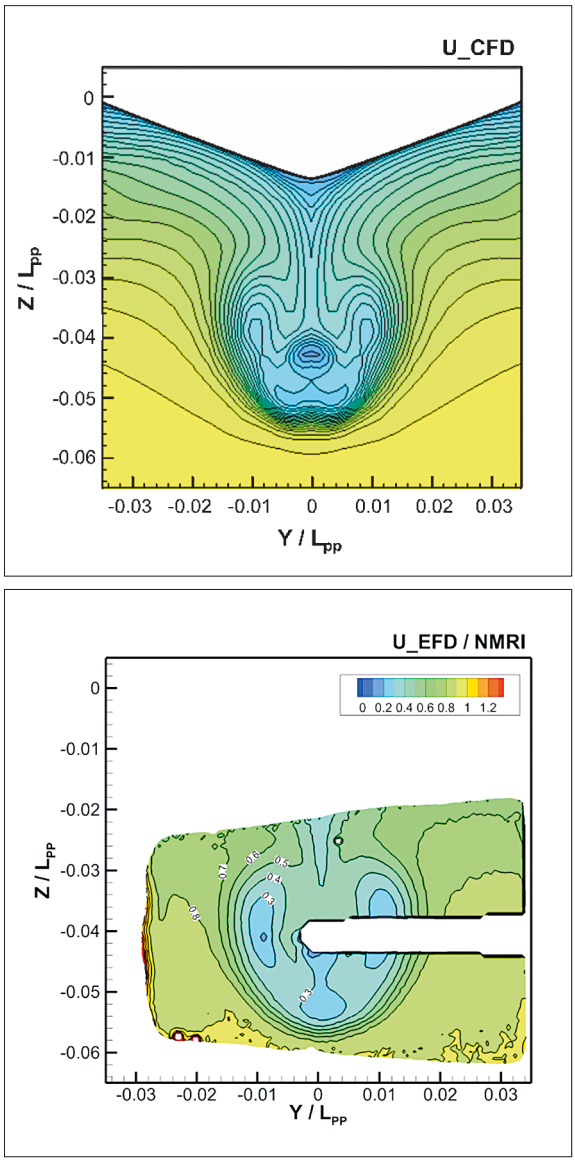

Fig. 17. Comparing computed axial velocity distributions in propeller's plane with EFD [21] in ship resistance condition

Comparing the axial velocity distributions in Fig. 17 reveals that the computed wake is in a reasonable agreement with the measured one.

In Fig. 18, the results of wake distribution demonstrate velocity acceleration and asymmetric flow configuration inside the propeller region due to propeller rotation.

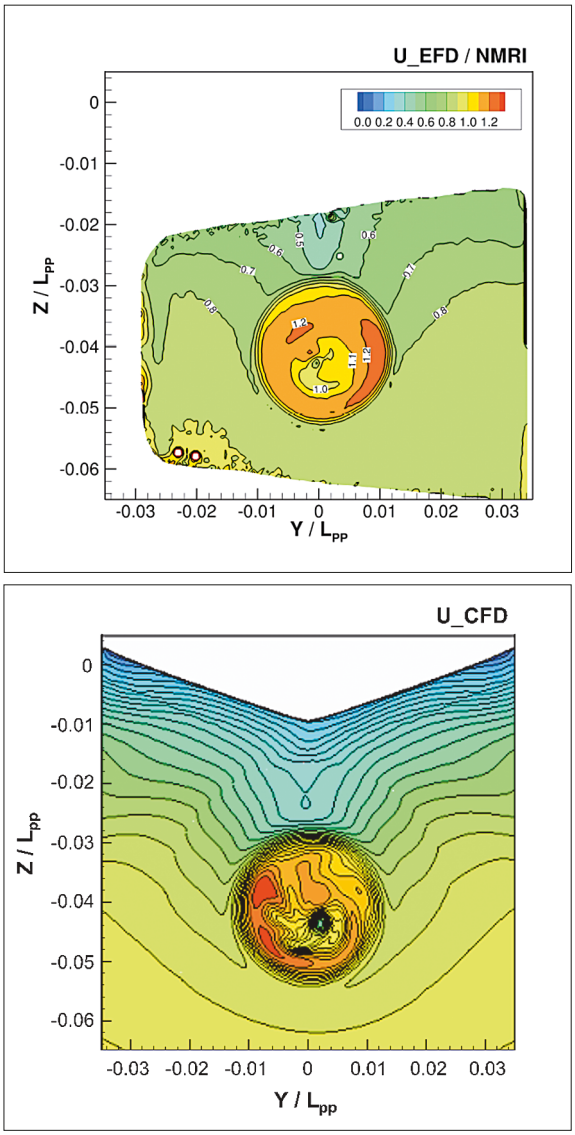

Fig. 18. Comparing computed axial velocity distributions in AP section with EFD [21] in self-propulsion condition

CONCLUSIONS

In the present study, the Unsteady RANS method has been applied to predict the coefficients of hull-propeller interaction for the JBC ship model. To obtain these coefficients, three case studies were analysed: ship resistance, propeller open-water, and self-propulsion simulations. In the resistance computations and in the self-propulsion simulation, the hull was free to trim and sink. In numerical computations of propeller open water characteristics, the rotating reference frame was used. For the propeller working behind the ship, the rigid body motion method was applied by using the sliding mesh technique.

The factors affecting the numerical accuracy of the obtained results, such as computational domain, time step, y+ value, mesh generation technique, and mesh dependency, were considered in this study.

The results of computations of individual components representing the interaction between the propeller and the ship hull, including thrust deduction (t), wake fraction (w_T), and relative rotative efficiency (η_R) showed good agreement with the experimental data. The error between computed and measured results was within 0.298 to 4.47%.

ACKNOWLEDGMENT

The authors are grateful to the Vietnam Maritime University for providing necessary research facilities during current research work.

REFERENCES

1. Tu, T.N., et al., *Numerical Study on the Influence of Trim On Ship Resistance In Trim Optimization Process*. Naval Engineers Journal, 2018. 130(4): p. 133–142.
2. Villa, D., S. Gaggero, and S. Brizzolara. *Ship Self Propulsion with different CFD methods: from actuator disk to viscous inviscid unsteady coupled solvers. in The10th International Conference on Hydrodynamics*. 2012.
3. Pacuraru, F., A. Lungu, and O. Marcu. *Self-Propulsion Simulation of a Tanker Hull. in AIP Conference Proceedings*. 2011. AIP.
4. Win, Y.N., et al., *Computation of propeller-hull interaction using simple body-force distribution model around Series 60 CB= 0.6*. Journal of the Japan Society of Naval Architects and Ocean Engineers, 2013. 18: p. 17–27.
5. Bugalski, T. and P. Hoffmann. *Numerical simulation of the self-propulsion model tests. in Second International Symposium on Marine Propulsors smp*. 2011.
6. Bekhit, A. *Numerical simulation of the ship self-propulsion prediction using body force method and fully discretized propeller model. in IOP Conference Series: Materials Science and Engineering*. 2018. IOP Publishing.
7. Seo, J.H., et al., *Flexible CFD meshing strategy for prediction of ship resistance and propulsion performance.* International Journal of Naval Architecture and Ocean Engineering, 2010. 2(3): p. 139–145.
8. Gokce, M.K., O.K. Kinaci, and A.D. Alkan, *Self-propulsion estimations for a bulk carrier.* Ships and Offshore Structures, 2018: p. 1–8.
9. Tran Ngoc Tu, N.M.C., *Comparison Of Different Approaches*

For Calculation Of Propeller Open Water Characteristic Using RANSE Method. Naval Engineers Journal, 2018. Volume 130, Number 1, 1 March 2018, pp. 105–111(7).

10. http://www.t2015.nmri.go.jp/jbc_gc.html.

11. http://www.t2015.nmri.go.jp/Instructions_JBC/instruction_JBC.html.

12. *ITTC 2011b Recommended procedures and guidelines 7.5-03-02-03*.

13. *CD-ADAPCO. User Guide STAR-CCM+, Version 13.02. 2018*.

14. Baltazar, J.M., D.R. Rijpkema, and J. Falcao De Campos. *Numerical studies for verification and validation of open-water propeller RANS computations. in Proceedings of the 6th International Conference on Computational Methods in Marine Engineering (Rome, Italy)*. 2015.

15. https://www.ittc.info/media/8169/75-03-03-01.pdf.

16. Chen, Z., *CFD investigation in scale effects on propellers with different blade area ratio*. 2015.

17. Wilcox, D.C., *Turbulence modeling for CFD*. Vol. 2. 1998: DCW industries La Canada, CA.

18. *ITTC-Quality Manual 7.5-03-01-01, 2008.*

19. https://ittc.info/media/1587/75-02-03-011.pdf.

20. Molland, A.F., S.R. Turnock, and D.A. Hudson, *Ship resistance and propulsion*. 2017: Cambridge university press.

21. http://www.t2015.nmri.go.jp/Presentations/Day1-AM2-JBC-TestData1-Hirata.pdf.

CONTACT WITH THE AUTHORS

Tran Ngoc Tu
e-mail: tutn.dt@vimaru.edu.vn

Vietnam Maritime University
Lay Tray, 1800 Hai Phong
Vietnam